



Pt nanoparticles entrapped in $\text{Al}_2\text{O}_3@\text{SBA-15}$ composites: Effective and recyclable catalysts for enantioselective hydrogenation of ethyl 2-oxo-4-phenylbutyrate

Xiaohong Li ^{*}, Haihong Wang, Huiyan Pan, Yi Meng Wang, Peng Wu

Shanghai Key Laboratory of Green Chemistry and Chemical Processes, Department of Chemistry, East China Normal University, 3663 North Zhongshan Road, Shanghai 200062, PR China



ARTICLE INFO

Article history:

Received 12 June 2014

Received in revised form

16 September 2014

Accepted 21 September 2014

Available online 26 September 2014

Keywords:

Enantioselective hydrogenation

Ethyl 2-oxo-4-phenylbutyrate

Pt catalyst

Cinchonidine

$\text{Al}_2\text{O}_3@\text{SBA-15}$ composites

Ultrasonic impregnation

ABSTRACT

Solid-state grinding, ultrasonic impregnation and conventional impregnation methods were adopted to synthesize mesoporous composites $\text{Al}_2\text{O}_3@\text{SBA-15}$ supported Pt catalysts for chiral hydrogenation of ethyl 2-oxo-4-phenylbutyrate after modified with cinchonidine. Compared with Pt/SBA-15 or Pt/alumina catalyst, Pt/ $\text{Al}_2\text{O}_3@\text{SBA-15}$ catalysts afforded better results when alumina loading in $\text{Al}_2\text{O}_3@\text{SBA-15}$ composites reached above 15 wt.%. Nevertheless, the catalytic performance of Pt/ $\text{Al}_2\text{O}_3@\text{SBA-15}$ catalysts was affected by preparation methods for $\text{Al}_2\text{O}_3@\text{SBA-15}$ composites. Ultrasonic impregnation of SBA-15 with an aqueous solution of aluminum nitrate led to uniformly dispersed $\text{Al}_2\text{O}_3@\text{SBA-15}$ composites and then enhanced the interaction between SBA-15 silica and alumina. Correspondingly, the Pt/ $\text{Al}_2\text{O}_3@\text{SBA-15}$ catalyst prepared by this method showed the best results (up to 11,928 h⁻¹ TOF and 87.9% ee) and could be reused for several times. Based on the spectroscopic characterizations, we deduced that the acidity of the composites, the Pt particle size and dispersion, and the electronic properties of Pt particles played vital roles in determining the catalytic performance.

© 2014 Elsevier B.V. All rights reserved.

1. Introduction

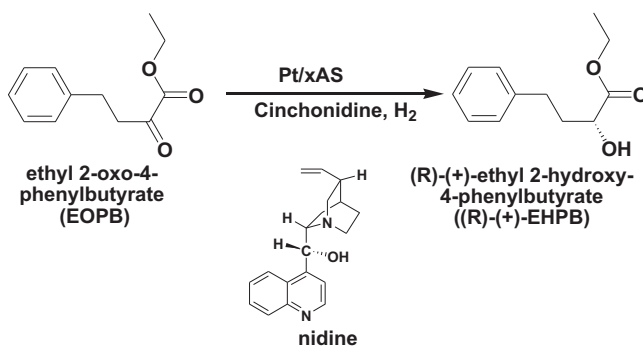
Heterogeneous enantioselective catalysis is a promising route for the production of enantiopure compounds because it has many benefits compared to other technologies [1]. Enantioselective hydrogenation of α -functionalized ketones to the corresponding chiral alcohols is an important chemical process owing to great application of chiral alcohols in synthesis of chiral drugs, pesticides, food additives and perfumes, etc. [2,3]. Since the discovery of asymmetric hydrogenation of α -ketoesters with cinchona alkaloid chirally modified Pt/ Al_2O_3 catalyst by Orito et al. [4–6], many scientists have taken extensive efforts to study this catalyst system and to explore new catalyst systems [7–15]. Nevertheless, most of supported Pt catalysts displayed catalytic properties inferior to the commercial Pt/ Al_2O_3 catalyst. A few exceptions arose recently. The Pt nanoparticles confined in the mesoporous alumina composites Al₂O₃@SBA-15 and the Pt nanocatalyst encapsulated within carbon nanotubes both showed a performance superior to well-known Pt/ Al_2O_3 in the enantioselective hydrogenation of α -ketoesters

under the similar reaction conditions [16,17]. Clearly, to the best of our knowledge, alumina-based material is still to be one of the most suitable supports for designing the supported Pt nanoparticle catalysts with a high enantioselectivity.

In our previous work, we prepared Al₂O₃@SBA-15 composites by incorporating the alumina precursor inside the mesopores of as-made mesoporous silica SBA-15 using a solvent-free solid-state grinding technique [16]. The Al₂O₃@SBA-15 composites retained the mesostructure of SBA-15 host, while the alumina was highly dispersed and uniformly coated on the silica walls. Furthermore, the Al₂O₃@SBA-15 composites proved to be the remarkable supports for Pt nanoparticles in the enantioselective hydrogenation of ethyl pyruvate; as a result, better catalytic performances were obtained on Pt/ $\text{Al}_2\text{O}_3@\text{SBA-15}$ catalysts compared with those obtained with the Pt catalysts supported on pure alumina or on pure SBA-15. Nevertheless, the solvent-free solid-state grinding method for preparation of the Al₂O₃@SBA-15 composites is still challengeable because it is very sensitive to humidity, room temperature and grinding time. It needs stringent requirements on surroundings and thus the repeatability of preparation of Al₂O₃@SBA-15 composites with the solvent-free solid-state grinding method cannot be guaranteed for each batch. Consequently, we have been devoting ourselves to exploring other methods to prepare the Al₂O₃@SBA-15

* Corresponding author. Tel.: +86 21 6223 8590; fax: +86 21 6223 8590.

E-mail address: xhli@chem.ecnu.edu.cn (X. Li).



Scheme 1. Heterogeneous enantioselective hydrogenation of ethyl 2-oxo-4-phenylbutyrate with Pt/xAS catalysts after chirally modified with cinchonidine.

composites to support Pt nanoparticles with high catalytic performance toward the enantioselective hydrogenation of α -ketoesters.

Herein, we reported our new progress in the enantioselective hydrogenation of another α -ketoesters, ethyl 2-oxo-4-phenylbutyrate (EOPB), as its hydrogenated product is an intermediate for ACE inhibitors (Scheme 1), catalyzed by the cinchonidine modified Pt catalysts supported on $\text{Al}_2\text{O}_3@\text{SBA-15}$ composites prepared by other methods, including ultrasonic impregnation method and stirring impregnation methods using different solvents. We found that the Pt catalysts supported on $\text{Al}_2\text{O}_3@\text{SBA-15}$ composites prepared by an ultrasonic impregnation method were most active toward the enantioselective hydrogenation of EOPB and could be recycled for at least seven times without obvious loss in conversion or enantioselectivity. Based on spectroscopic characterization results, the possible reasons were also discussed.

2. Experimental

2.1. Preparation of $\text{Al}_2\text{O}_3@\text{SBA-15}$ composites

SBA-15 was prepared according to Ref. [18]. After getting the white powder of as-made SBA-15, it was calcined in air at 823 K for 5 h to remove the template. The $\text{Al}_2\text{O}_3@\text{SBA-15}$ composites were prepared through five different post-synthesis routes.

2.1.1. Route I (UIW method)

An ultrasonic impregnation method was applied to load alumina inside the mesopores of SBA-15 [19]. The required alumina precursor $\text{Al}(\text{NO}_3)_3 \cdot 9\text{H}_2\text{O}$ was firstly dissolved in deionized water. Then, a certain amount of SBA-15 was added into the above mixture and followed by an ultrasonic treatment for 4–6 h. After that, the mixture was evaporated and dried thoroughly at 323 K. The resultant powder was calcined in air at 823 K for 5 h before use.

2.1.2. Route II (SIW method)

The required alumina precursor $\text{Al}(\text{NO}_3)_3 \cdot 9\text{H}_2\text{O}$ was firstly dissolved in deionized water. Then, the mesoporous silica SBA-15 was impregnated with the above mixture with stirring at room temperature for 12 h. After that, the powder was filtered and dried naturally at 323 K. The resultant powder was calcined in air at 823 K for 5 h before use.

2.1.3. Route III (SIH method)

The required amount of another alumina precursor aluminum isopropoxide was firstly dispersed in dry hexane, then a certain amount of SBA-15 was added [20]. The resulting mixture was stirred at room temperature for 12 h. Then, the powder was filtered, washed with dry hexane, and dried at room temperature in

Table 1
Specifications of different preparation methods for $\text{Al}_2\text{O}_3@\text{SBA-15}$ composites.

Abbreviation	Al source	Methods	Solvent
SSG	$\text{Al}(\text{NO}_3)_3 \cdot 9\text{H}_2\text{O}$	Solid-State-Grinding	None
UIW	$\text{Al}(\text{NO}_3)_3 \cdot 9\text{H}_2\text{O}$	Ultrasonic-Impregnation	Water
SIW	$\text{Al}(\text{NO}_3)_3 \cdot 9\text{H}_2\text{O}$	Stirring-Impregnation	Water
SIH	$\text{Al}(\text{i-OPr})_3$	Stirring-Impregnation	Hexane
SIF	$\text{Al}(\text{i-OPr})_3$	Stirring-Impregnation	Furfuryl alcohol

air. The resultant powder was calcined in air at 823 K for 5 h before used as support.

2.1.4. Route IV (SIF method)

Al was firstly grafted into SBA-15 with a Si/Al molar ratio of 10 to synthesize Al-SBA-15 [21,22]. Then, a furfuryl alcohol (FA) solution of aluminum isopropoxide was used to immerse Al-SBA-15 via an incipient impregnation method to prepare $\text{Al}_2\text{O}_3@\text{SBA-15}$ composites. After heating at 333 K for 2 h to make FA polymerize, the mixture was evaporated under vacuum to volatilize the rest of FA at 333 K for 12 h. Then, the powder was calcined under nitrogen atmosphere at 823 K for 6 h to make the polymerized FA carbonize. The resultant black materials were calcined in air at 823 K for 6 h to remove carbon, and finally the $\text{Al}_2\text{O}_3@\text{SBA-15}$ composites with highly dispersed alumina were obtained.

2.1.5. Route V (SSG method)

For comparison, a series of $\text{Al}_2\text{O}_3@\text{SBA-15}$ composites with different alumina loadings were prepared using the solvent-free solid-state grinding method according to Ref. [16] as well.

For the $\text{Al}_2\text{O}_3@\text{SBA-15}$ composites prepared using different routes, the amount of Al sources was adjusted to yield the desirable Al_2O_3 loadings of 15 wt.%, 25 wt.% and 35 wt.% in the final $\text{Al}_2\text{O}_3@\text{SBA-15}$ composites. According to the different routes, the resultant $\text{Al}_2\text{O}_3@\text{SBA-15}$ composites were denoted as $x\text{AS}$ -SSG/UIW/SIW/SIH/SIF, where x represents the alumina loading (wt.%), A represents Al_2O_3 , S represents SBA-15, SSG represents the solid-state-grinding method, UIW represents the ultrasonic-impregnation with water as solvent, SIH represents stirring impregnation with hexane as solvent, SIF represents stirring impregnation with FA as solvent. For convenience, the detailed preparation specifications for $\text{Al}_2\text{O}_3@\text{SBA-15}$ composites are listed in Table 1. The detailed preparation procedures are also illustrated in Fig. 1.

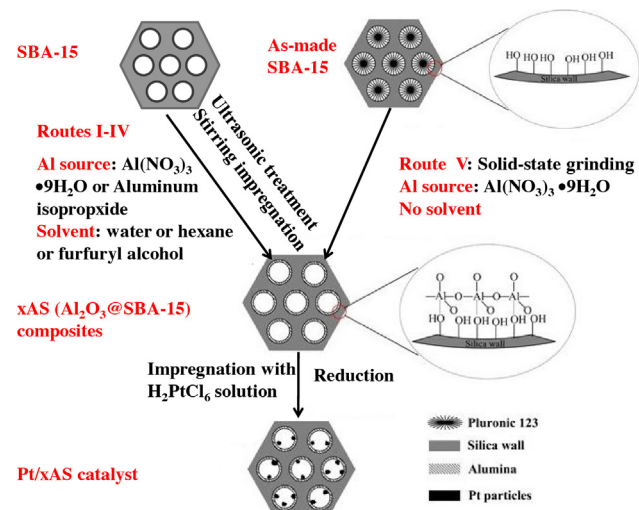


Fig. 1. Preparation of xAS composites and Pt/xAS catalysts.

2.2. Preparation of Pt/Al₂O₃@SBA-15 catalysts

The 5 wt.% Pt/xAS catalysts were prepared mainly according to Ref. [23]. The xAS composites were impregnated with H₂PtCl₆ solution dissolved in a 1:1 (v/v) mixture of water and ethanol. According to desirable 5 wt.% Pt loading, the required volume of H₂PtCl₆ solution with a concentration of 14.8 mg Pt/ml was calculated firstly and then about 3–4 mL of water and ethanol mixed solvent (1:1, v/v) was added to make the support immerse well in the solution. After stirring for 6 h, the mixture was evaporated to remove the excess solvent, followed by drying at 393 K overnight. The catalyst precursor was then directly reduced in an aqueous solution of sodium formate by refluxing at 363 K for 2 h. To make the catalyst precursor immerse well in the solution, about 20 mL water was added. Finally, the mixture was washed by plenty of water to remove chlorine ions and dried at 353 K overnight.

2.3. Characterization of xAS composites and Pt/xAS catalysts

The X-ray diffraction (XRD) patterns of samples were collected on a Bruker D8 Advance instrument using Cu-K α radiation. The nitrogen adsorption–desorption isotherms were measured at 77 K on a Quantachrome Autosorb-3B system, after the samples were evacuated for 10 h at 473 K. The BET specific surface area was calculated using adsorption data in the relative pressure range from 0.05 to 0.30. The pore size distributions were calculated from the analysis of the adsorption branch of the isotherm using the BJH algorithm. The transmission electron microscopy (TEM) images were taken on an FEI Tecnai G2-TF30 microscope at an acceleration voltage of 300 kV. The scanning electron microscopy (SEM) images were taken on a Hitachi S4800 electron microscope with an acceleration voltage of 20 kV.

CO chemisorption of samples was measured at 308 K on a Quantachrome CHEMBET-3000 pulse chemisorption analyzer after the samples were pretreated in a 5 vol.% H₂/95 vol.% Ar flow at 673 K for 2 h. The degree of dispersion and the mean particle size (cubic model) were estimated from the measured CO uptake, assuming a cross-sectional area for a surface platinum atom of $8.0 \times 10^{-20} \text{ m}^2$ and a stoichiometric factor of one, using nominal platinum concentrations.

The surface electronic state of platinum particles was examined by diffuse reflectance infrared Fourier-transform spectroscopy (DRIFTS) using CO as probe molecules. The analysis was conducted with a Nicolet NEXUS 670 spectrometer. The catalyst sample was pretreated in a 5 vol.% H₂/95 vol.% Ar stream at 673 K for 2 h, and then was purged with He for 30 min. When the sample was cooled down to 308 K, CO was introduced into the IR cell until the adsorption was saturated. Then, the sample was flushed with a He flow before the spectrum was recorded.

The surface electronic state of Pt was also evaluated using X-ray photoelectron spectroscopy (XPS) measurements with a Thermo Fisher Scientific ESCALAB 250Xi spectrometer with Al K α radiation (1486.6 eV) as incident beam with a monochromator. All the samples were pretreated in flowing hydrogen at 673 K for 1 h in a reactor attachment of the XPS spectrometer. All the spectra were obtained at room temperature, and the binding energies of elements were referenced to the adventitious C1s peak at 284.8 eV. The spectra shown in the figures have been corrected by subtraction of a Shirley background. Spectral fitting and peak integration was done using the XPSPEAK software.

The acidic properties of the xAS composites were characterized by IR spectroscopy, using pyridine as probe molecules. The infrared spectra of xAS and Pt/xAS samples were also recorded with a Nicolet NEXUS 670 Fourier transform infrared spectrometer. Before the IR investigation, the samples were pressed into self-supported wafers and activated under vacuum at 773 K for 1 h. When the cell was

cooled down to room temperature, the samples were exposed to pyridine vapor for 20 min. After degassing at 573 K for 1 h, the spectrum was recorded to characterize the acidity of the samples. ²⁹Si and ²⁷Al MAS NMR spectra were recorded at 400 MHz on a Varian VNMRS400WB spectrometer equipped with a magic angle spin probe at room temperature. The leached amount of Pt atoms into solution after reaction were detected with a Thermo Elemental IRIS Intrepid II XSP inductively coupled plasma-atomic emission spectroscopy (ICP-AES).

2.4. Catalytic tests

In a typical reaction, 0.1 g 5 wt.% Pt/xAS catalyst was pre-treated under a hydrogen flow at 673 K for 2 h before use. The catalyst was then mixed with 20 mL acetic acid, 10 mg cinchonidine and 1 mL EOPB. The mixture was subsequently transferred to a 100 mL autoclave. The hydrogenation reaction began with stirring (1000 rpm) at room temperature after 4.0 MPa of hydrogen was introduced into the autoclave. The reaction was stopped after 15 min and the products were analyzed by GC-FID (GC-2014, Shimadzu Co.) equipped with a chiral capillary column (HP19091G-B213, 30 m × 0.32 mm × 0.25 m, Agilent Co.). The optical yield was expressed as the enantiomeric excess (% ee) of (R)-(+)-ethyl lactate: ee (%) = ([R] - [S])/([R] + [S]) × 100.

After each run, the catalyst was recovered by centrifugation and washed with fresh solvent for several times. Then, fresh reactant, solvent and cinchonidine were charged to the autoclave together with the recovered catalyst to conduct the next run reaction.

3. Results and discussion

3.1. Structural characterization of xAS composites and Pt/xAS catalysts

The small angle XRD patterns of xAS composites and the resultant Pt/xAS catalysts are shown in Fig. S1 in the Supplementary data. The xAS composites and the resultant Pt/xAS catalysts all displayed the typical (1 0 0), (1 1 0), and (2 0 0) diffractions associated with the hexagonal space group p6mm structure [18]. Compared with SBA-15 host, the diffraction angles for the Al₂O₃@SBA-15 composites shifted slightly to higher region, probably due to the shrinkage during the re-calcination process [24]. This demonstrates that inclusion of alumina inside SBA-15 mesopores and even loading of Pt nanoparticles did not destroy the structure of SBA-15 host. This also implies that the xAS composites possess a strong hydrothermal stability as the Pt/xAS catalysts suffered from impregnation with the acidic H₂PtCl₆ solution and were refluxed at a high temperature in an aqueous solution of sodium formate in order to reduce the Pt precursors.

The mesoporous structure of xAS composites and the resultant Pt/xAS catalysts was further confirmed by the nitrogen adsorption–desorption isotherms. As displayed in Figs. S2 and S3 in the Supplementary data, the xAS composites and the Pt/xAS catalysts exhibited typical type IV isotherms and showed clear H1-type hysteresis loops in the range of $P/P_0 = 0.5\text{--}0.8$. Nevertheless, the mesopores of SBA-15 host were partly plugged by introduced alumina in some cases, especially for those with higher loading of alumina; as a result, the pore volumes were correspondingly decreased. Table 2 lists the relevant physicochemical properties of all the xAS composites. The BET specific surface area and the pore volume for all the xAS composites, regardless of the different preparation method, decreased with increasing alumina loading compared with the SBA-15 host, because the more alumina was included, the more surface area and the more pore volume of the SBA-15 host was occupied. For the xAS composites, the BET specific

Table 2

The relevant physicochemical data for SBA-15 host and xAS composites.

Entry	Samples	Al ₂ O ₃ loading (wt.%)	S _{BET} ^a (m ² g ⁻¹)	Pore volume ^a (cm ³ g ⁻¹)	Pore size ^a (nm)
1	SBA-15	0	830	1.04	8.1
2	15AS-SSG	15	499	0.76	8.0
3	25AS-SSG	25	445	0.74	7.9
4	35AS-SSG	35	363	0.58	7.8
5	15AS-UIW	15	471	0.84	6.8
6	25AS-UIW	25	401	0.69	6.7
7	35AS-UIW	35	307	0.47	6.8
8	15AS-SIW	15	503	0.75	7.4
9	25AS-SIW	25	380	0.57	7.3
10	35AS-SIW	35	287	0.44	7.3
11	15AS-SIH	15	498	0.91	7.4
12	25AS-SIH	25	509	0.83	7.7
13	35AS-SIH	35	336	0.64	7.4
14	35AS-SIF	35	369	0.58	6.7
15	Al ₂ O ₃	100	232	0.51	4.7

^a Determined by N₂ adsorption.

surface area was in the range of 287–509 m² g⁻¹, while the pore volume varied from 0.44 to 0.91 cm³ g⁻¹. When converted to per gram of silica SBA-15, the specific surface area of the xAS composites almost converged toward values between 500 and 600 m² g⁻¹, indicating that the pore system of SBA-15 has been modified by alumina introduction more deeply than just by deposition of alumina layers in cylindrical pores. The microporosity of SBA-15 was mostly clogged and even the mesopores were partly plugged in some cases. Additionally, the introduction of aluminum salts also resulted in part insertion of aluminum into the framework of SBA-15; as a result, there were some Al^V species, which could be confirmed by ²⁷Al NMR and IR results of Si-OH stretching vibration region (the detailed NMR and IR characterizations will be discussed in the next parts), regardless of different preparation methods.

The pore size of the xAS composites calculated from the Barrett–Joyner–Halenda (BJH) pore size distributions also decreased with increasing alumina loading. For the xAS composites prepared by SIW, SIH and SSG methods, the pore size distributions almost centered at 7.5 nm, whereas for the xAS-UIW series, the pore size was a little smaller. This might imply that alumina in the xAS-UIW series were mostly located inside the mesoporous channels of SBA-15. The relevant physicochemical parameters for the Pt/xAS catalyst are also displayed in Table 3. Normally, the BET specific surface area of the Pt/xAS catalyst decreased with the increase of alumina loading and the Pt/xAS catalyst had a specific surface area of about 300–400 m² g⁻¹.

The morphology of xAS composites and Pt/xAS catalysts was also characterized using SEM. As can be seen from the SEM images for part of xAS composites and Pt/xAS catalysts in Fig. S4 (see Supplementary data), the alumina was uniformly dispersed along the mesoporous channels of the SBA-15 host. With the increase of alumina loading, the outer surface became rough more or less. If the alumina loading reached 35 wt.%, some alumina grains could be clearly observed (see Fig. S4e for the SEM image of 35AS-UIW).

The alumina phase and Pt particle dispersion of Pt/xAS catalysts were firstly characterized by wide-angle XRD. Compared with the pure Al₂O₃-supported Pt catalysts, no distinct XRD patterns assignable to the crystalline alumina phase were observed for the Pt/xAS catalysts, indicating that alumina guest was well dispersed into the SBA-15 host in spite of the preparation method, even if the Al₂O₃ loading reached 35 wt.% (see Fig. S5 in the Supplementary data). It is in good accordance with the SEM images. SBA-15 containing straight cylindrical pores with 2-D arrangement would probably lead to homogeneous distribution of the alumina precursor particles along the channels [25]. As also observed from the wide-angle XRD patterns, the 5 wt.% Pt/SBA-15, Pt/Al₂O₃ and Pt/xAS catalysts showed somewhat diffraction peaks indexed as Pt(111),

and even Pt(200) and Pt(220) in some cases, suggesting that the population of Pt particles larger than 3 or 4 nm cannot be negligible. According to Scherrer formula, the larger Pt particle size could reach 6–7 nm.

The Pt particle size and distribution of Pt/xAS catalysts were further characterized by TEM. Fig. 2 displays the TEM images of representative Pt/xAS catalysts such as Pt/xAS-UIW series, Pt/35AS-SIF and Pt/Al₂O₃ catalysts. It is clearly observed that the mesoporous ordered structure of xAS composites was well preserved. Moreover, the Pt nanoparticles were highly dispersed on the support. In addition, there were a few alumina grains located outside the mesoporous channels (see Fig. 2d for the TEM image of the Pt/35AS-SIF catalyst), although the XRD pattern of this catalyst did not show the diffraction peak assignable to crystalline alumina phase. CO chemisorption was also employed to calculate the Pt particle size and distribution. As already contained in Table 3, the calculated results based on the measured CO chemisorption are consistent with the TEM results. For instance, the Pt/xAS-UIW series catalysts had relatively smaller Pt particle size (2.3–2.4 nm) when compared with the others. The Pt/xAS catalysts, regardless of the preparation methods for the xAS composites, had an average Pt particle size of 2.9 ± 0.6 nm.

3.2. Catalytic performances of Pt/xAS catalysts for chiral hydrogenation of EOPB

The catalytic performance of Pt/xAS catalysts was tested for the enantioselective hydrogenation of EOPB after modification with chiral modifier cinchonidine. It has been discovered that (R)-(+)-ethyl-2-hydroxy-4-phenylbutyrate, the hydrogenation product of asymmetric hydrogenation of EOPB, can be widely used in the preparation of chiral medicine Enalapril, which then can be used in therapy of many important symptoms such as hypertension and myocardial infarction [26].

Table 4 lists the results for the asymmetric hydrogenation of EOPB with the cinchonidine chirally modified Pt/xAS catalysts. The cinchonidine-modified Pt/SBA-15 catalyst only afforded 1.3% conversion and 21.9% ee within 15 min (Table 4, entry 1). In contrast, the cinchonidine-modified Pt/alumina catalyst gave 60.3% conversion and 75.4% ee value under the same conditions (Table 4, entry 2).

When alumina was coated into SBA-15 to form the xAS composites, the Pt/xAS catalysts gave superior catalytic performance to Pt/SBA-15 catalyst. Generally, with increase of alumina loading in the xAS composites for the same series catalyst, the catalytic results obtained with the Pt/xAS catalysts were increased correspondingly. For instance, the Pt/15AS-SIW, Pt/25AS-SIW and Pt/35AS-SIW

Table 3

Relevant physicochemical parameters for Pt/xAS catalysts.

Entry	Catalyst	Al ₂ O ₃ content (wt.%)	S _{BET} ^a (m ² g ⁻¹)	V _p ^a (cm ³ g ⁻¹)	D _p ^a (nm)	Pt size ^b (nm)
1	Pt/15AS-SSG	15	386	0.67	7.7	n.d.
2	Pt/25AS-SSG	25	395	0.83	8.4	3.5
3	Pt/35AS-SSG	35	335	0.77	8.1	n.d.
4	Pt/15AS-UIW	15	398	0.66	6.8	2.3
5	Pt/25AS-UIW	25	337	0.56	6.2	2.3
6	Pt/35AS-UIW	35	296	0.79	5.8	2.4
7	Pt/15AS-SIW	15	433	0.73	6.8	n.d.
8	Pt/25AS-SIW	25	345	0.60	6.3	2.9
9	Pt/35AS-SIW	35	333	0.76	6.7	n.d.
10	Pt/15AS-SIH	15	386	0.76	7.3	n.d.
11	Pt/25AS-SIH	25	357	0.64	6.8	2.7
12	Pt/35AS-SIH	35	316	0.64	6.8	n.d.
13	Pt/35AS-SIF	35	313	0.65	6.2	2.8
14	Pt/Al ₂ O ₃	100	217	0.42	3.9	n.d.

n.d.: not determined.

^a Determined by N₂ adsorption.^b Average Pt particle size was determined by CO chemisorption.

catalysts gave 31.9% conversion with 76.3% ee, 80.5% conversion with 77.0% ee, and 84.1% conversion with 78.3% ee, respectively (**Table 4**, entries 3–5). The Pt/xAS-SIH series, the Pt/xAS-SSG series and the Pt/xAS-UIW series also showed the similar trend under the same conditions. As a result, the Pt/xAS catalysts, especially for the Pt catalysts supported on xAS composites with an alumina loading higher than 25 wt.%, were more active than the Pt/Al₂O₃ catalyst under the same conditions.

Besides the alumina loading, the preparation methods employed for the xAS composites also played an important role in determining the catalytic performance of the resultant Pt/xAS catalysts. For instance, the Pt/15AS-SIW catalyst, of which the support 15AS was prepared via a traditional stirring impregnation using water as solvent, gave 31.9–84.1% conversions with 76.3–78.3% ee values within 15 min (**Table 4**, entries 3–5), quite higher than that afforded by the Pt/SBA-15 catalyst. The Pt/xAS-SIH series catalysts, supported on xAS composites prepared through

a stirring impregnation method using hexane as solvent, showed similar results to those obtained with the Pt/xAS-SIW series, except that slightly higher conversions (up to 95.6%) were achieved with similar enantioselectivities (**Table 4**, entries 6–8).

When the xAS composites were fabricated by a solvent-free solid-state grinding method, the resultant Pt/xAS-SSG series catalyst exhibited much better catalytic performance particularly in terms of conversions of EOPB. Nearly 70% conversion was obtained within 15 min on the chirally modified Pt/15AS-SSG catalyst; although the ee value was a little lower (**Table 4**, entry 9). If the alumina loading in the composites was further increased, the catalytic performance of the Pt/xAS-SSG catalysts was further enhanced as well. About 94% conversion and higher than 80% ee value were achieved with the Pt/35AS-SSG catalyst within 15 min (**Table 4**, entry 11).

When the xAS composites were prepared using the ultrasonic impregnation method, the composites supported Pt catalysts gave the highest results among all of the Pt/xAS catalysts. The asymmetric hydrogenation of EOPB could be almost finished, obtaining 97.7–98.1% conversions within 15 min with cinchonidine-modified Pt/xAS-UIW series catalysts, even for the one supported on the composites with the lowest alumina loading, Pt/15AS-UIW (**Table 4**, entries 12–14).

Taking into account that the conversions were already close to 100%, it seemed that 15 min was too long to distinguish the difference between the Pt/xAS-UIW catalysts with different alumina loadings. In order to compare the catalytic performance between the Pt/xAS-UIW catalysts with different alumina loadings clearly, the reaction time was cut down to 5 min. To our delight, the Pt/15AS-UIW catalyst afforded 66.5% conversion with 82.0% ee value within 5 min (**Table 4**, entry 15). With the increase of alumina loading to 25 wt.% and 35 wt.% in the xAS-UIW composites, the chirally-modified Pt/25AS-UIW and Pt/35AS-UIW furnished 88.9% conversion with 83.7% ee value and 95.9% conversion and 85.1% ee, respectively (**Table 4**, entries 16–17).

Moreover, the reaction parameters including reaction time, catalyst and substrate dosage were also further optimized in order to greatly take advantage of the potential of the Pt/35AS-UIW catalyst. Although the reaction time was further shortened to 3 min, a conversion of 85% of EOPB with 84% ee value was still afforded by the Pt/35AS-UIW catalyst (**Table 4**, entry 18). If the catalyst dosage was decreased to a half, a similar conversion of 96.8% was achieved within the same reaction time (**Table 4**, entry 19). When a twice amount of EOPB was added, an 83.2% conversion was obtained within 5 min (**Table 4**, entry 20). In addition, in a certain recipe containing a half dosage of catalyst and about twice amount of

Table 4Conversions of EOPB and ee values of (R)-(+)–EHPB obtained with the cinchonidine-modified Pt/xAS catalysts^a.

Entry	Catalyst	t (min)	Conv. (%)	ee (%)
1	Pt/SBA-15	15	1.30	27.9
2	Pt/Al ₂ O ₃	15	60.3	75.4
3	Pt/15AS-SIW	15	31.9	76.3
4	Pt/25AS-SIW	15	80.5	77.0
5	Pt/35AS-SIW	15	84.1	78.3
6	Pt/15AS-SIH	15	30.4	74.0
7	Pt/25AS-SIH	15	90.6	81.9
8	Pt/35AS-SIH	15	95.6	78.7
9	Pt/15AS-SSG	15	68.7	69.5
10	Pt/25AS-SSG	15	89.1	78.3
11	Pt/35AS-SSG	15	93.9	80.2
12	Pt/15AS-UIW	15	97.7	81.0
13	Pt/25AS-UIW	15	98.0	82.2
14	Pt/35AS-UIW	15	98.1	83.1
15	Pt/15AS-UIW	5	66.5	82.0
16	Pt/25AS-UIW	5	88.9	83.7
17	Pt/35AS-UIW	5	95.9	85.1
18	Pt/35AS-UIW	3	85.0	84.1
19	Pt/35AS-UIW	5	96.8 ^b	87.9
20	Pt/35AS-UIW	5	83.2 ^c	85.0
21	Pt/35AS-UIW	5	58.6 ^d	85.6
22	Pt/35AS-SIF	15	97.3	85.6

^a Reaction conditions: 0.1 g Pt/xAS catalyst; 0.01 g cinchonidine; 1 mL EOPB (5.49 mmol); 20 mL acetic acid; 4.0 MPa H₂; room temperature; 1200 rpm.^b 0.05 g catalyst.^c 2 mL EOPB (10.98 mmol).^d 0.05 g catalyst, 10 mmol EOPB.

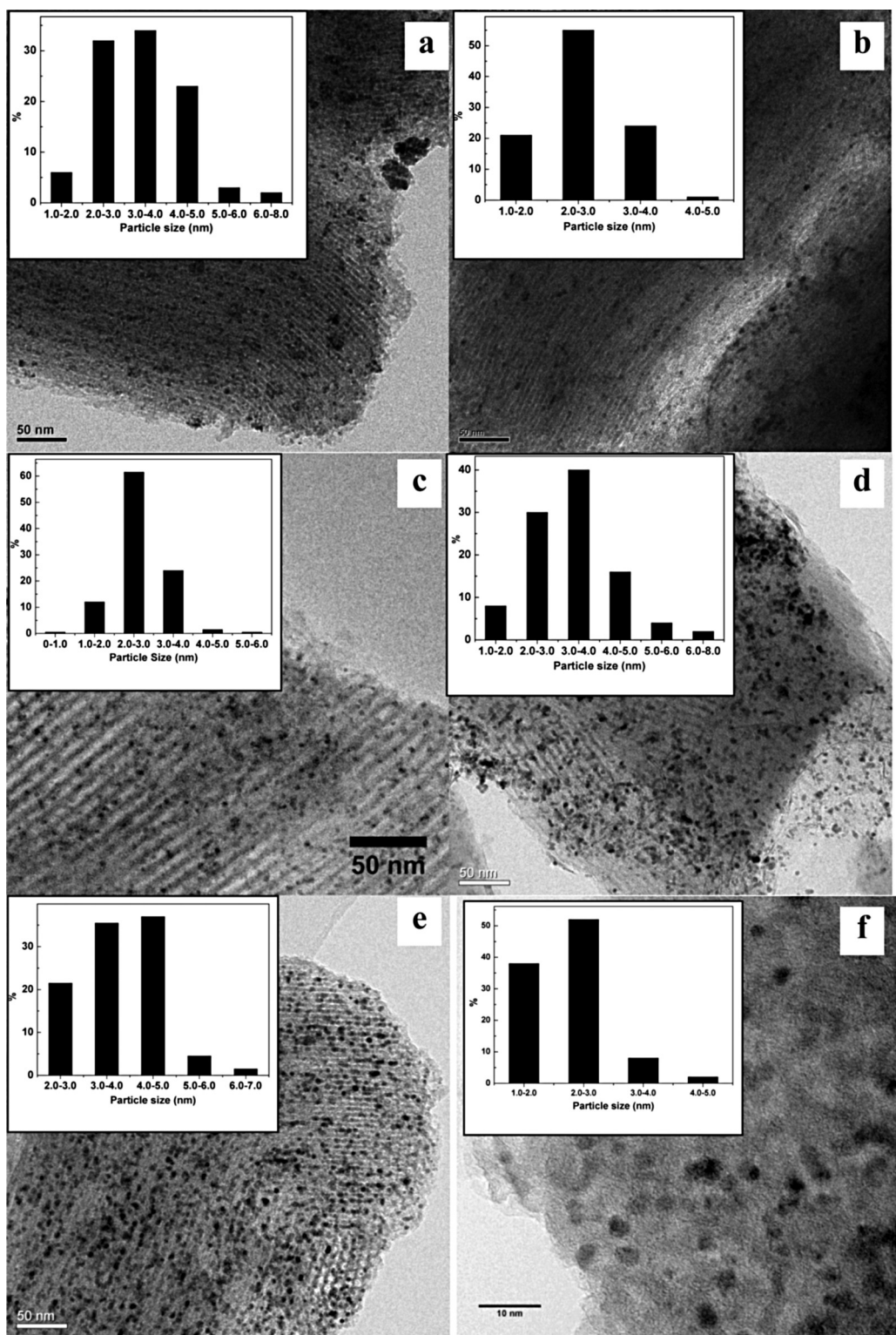


Fig. 2. TEM images and Pt particle size distribution of (a) Pt/15AS-UIW; (b) Pt/25AS-UIW; (c) Pt/35AS-UIW; (d) Pt/35AS-SIF; (e) the used Pt/35AS-UIW catalyst after eight cycles; (f) Pt/Al₂O₃.

substrate, close to 60% conversion was provided, furnishing a TOF up to 11,928 h⁻¹ (Table 4, entry 21).

In summary, the more alumina coated into SBA-15 in the xAS composites, the higher catalytic results obtained with the cinchonidine-modified Pt/xAS catalysts for the asymmetric hydrogenation of EOPB, no matter whatever method adopted to prepare the xAS composites. Furthermore, both the conversions and ee

values obtained with the Pt/xAS catalysts were much higher than that furnished with the Pt/SBA-15 catalyst. When compared with the results obtained with the Pt/Al₂O₃ catalyst, the Pt/xAS catalysts also exhibited higher catalytic results when the alumina loading in the xAS composites reached 25 wt.%. Among the four series Pt/xAS catalysts, the Pt/xAS-UIW series catalysts were superior to other three series under the same conditions. Additionally, it is worthy

of note that the Pt/35AS-SIF catalyst, of which the 35AS-SIF composites were prepared via a special route through impregnating Al-SBA-15 with an FA solution of aluminum isopropoxide, also gave excellent results, obtaining a 97.3% conversion and 85.6% ee value (Table 4, entry 22).

3.3. The reusability of Pt/xAS catalysts for the asymmetric hydrogenation of EOPB

The reusability of Pt/xAS catalyst was also an important matter to consider. Therefore, we investigated the reusability of chirally modified Pt/xAS catalysts toward the chiral hydrogenation of EOPB. Fig. 3 shows conversions and ee values against number of runs obtained with the Pt/25AS-SSG, Pt/35AS-SIF and Pt/35AS-UIW catalysts within 15 min, respectively. The Pt/25AS-SSG catalyst could be used for more than five times without distinct loss in activity. The activity was gradually declined after five runs (Fig. 3A). For the Pt/35AS-SIF catalyst, the similar recycling manner was displayed in Fig. 3B. To our excitement, the Pt/35AS-UIW catalyst could be recycled for at least seven times without obvious loss in activity compared with the other two catalysts (Fig. 3C). Since fresh cinchonidine was supplemented in each run, the enantioselectivity was maintained almost a same level upon several times re-use (80–83% ee).

To make clear the reason for the gradual decrease in activity with the Pt/xAS catalysts, the used catalyst was characterized in detail. Firstly, the collected catalysts were washed with fresh solvent, dried at 353 K overnight and weighed. To our surprise, the weight loss during each reaction cycle could not be neglected, as a total 44.2% weight was lost for the Pt/25AS-SSG catalyst after nine reaction cycles. For the used Pt/35AS-UIW catalyst, only 63% weight was retained after eight cycles. The tremendous weight loss for both the Pt/25AS-SSG and the Pt/35AS-UIW catalysts would inevitably result in a gradual decrease in catalyst activity. Even though the catalyst amount was gradually lost during the reaction, the catalytic performance was remained roughly the same, particularly for the first reaction runs, suggesting that the reaction may take place so rapidly on a minor fraction of the Pt particles that the measured rate heavily depends on the diffusion rate. Secondly, the filtrate was detected using ICP-AES technique to examine the leached Pt atoms because the Pt leaching also might be another important reason for the decreased catalyst activity. About 4.3% of Pt atoms were leached to filtrate for the Pt/25AS-SSG catalyst. While for the Pt/35AS-UIW catalyst, the Pt leaching was below the detection limit. This also implies that the interaction of Pt nanoparticles and the composites is strong so that Pt nanoparticles can be stabilized by the composites prepared by the UIW method.

Thirdly, the morphology of Pt/xAS catalyst was also characterized using SEM and TEM. As also displayed in Figs. S4h and S4i in the Supplementary data, the morphologies of the used Pt/35AS-SIF and the used Pt/35AS-UIW catalyst changed a lot after several reaction cycles compared with those of the fresh catalysts. In both cases, the alumina was attacked by acetic acid during reaction and moved off from the mesoporous channels of SBA-15 to form feather-like (Fig. S4h) or sheet-like flakes (Fig. S4i). The XRD pattern of the used catalyst (not shown) proved that the used Pt/35AS-UIW catalyst contained basic aluminum acetate ($\text{Al(OH)}(\text{CH}_3\text{COO})_2$), which was probably formed through a reaction of alumina with acetic acid during the several reaction cycles. It would affect the mass transportation undoubtedly. In addition, the Pt nanoparticles were aggregated to form relatively larger particles during recycling experiment. As also shown in Fig. 2e, the Pt particle size distribution for the used Pt/35AS-UIW catalyst was centered at 3–5 nm, while the fresh catalyst had an average Pt particle size of 2.4 nm. Certainly, the slightly enlarged Pt particle size also contributed to the gradual decrease in catalyst activity.

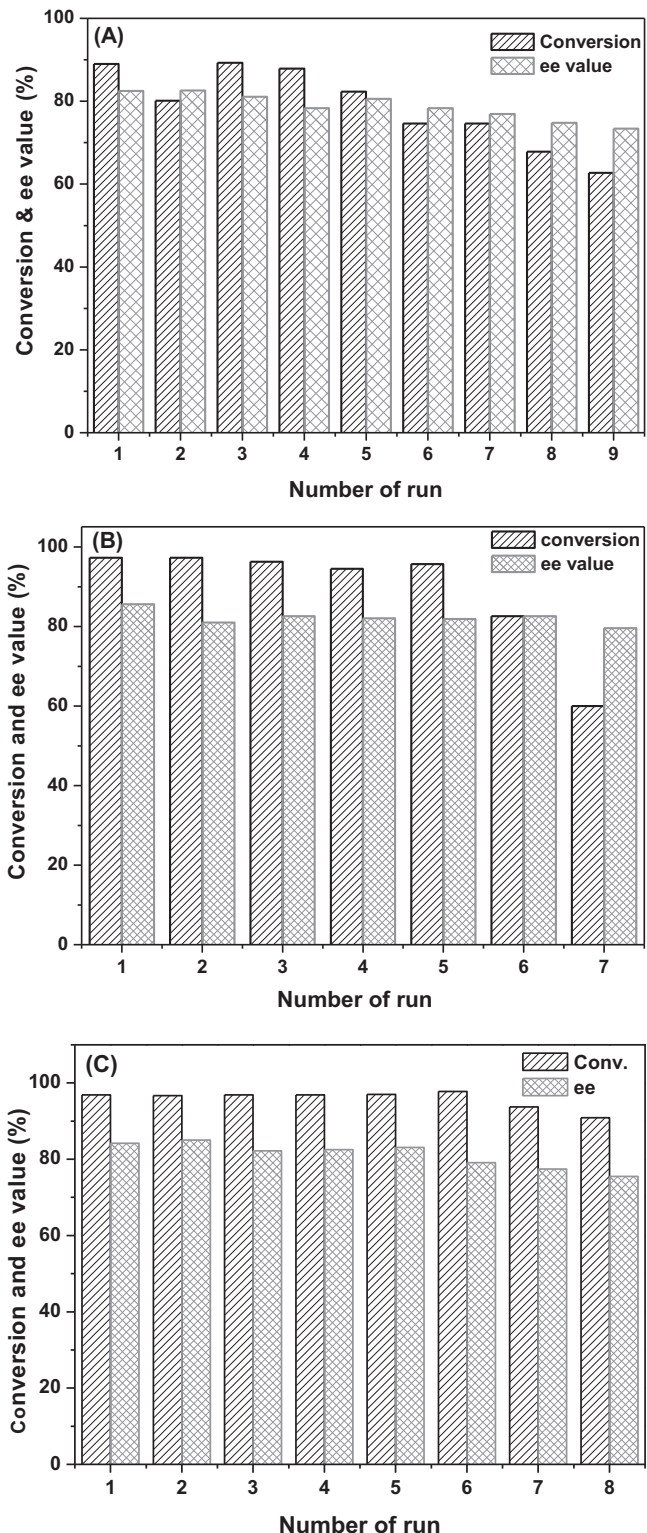


Fig. 3. The reusability of (A) Pt/25AS-SSG catalyst, (B) Pt/35AS-SIF catalyst and (C) Pt/35AS-UIW catalyst. Reaction conditions are identical to Table 3.

Nevertheless, when compared with the reusability of Pt catalyst supported on bare alumina, the reusability of Pt/xAS catalysts was greatly improved. For the $\text{Pt}/\text{Al}_2\text{O}_3$ catalyst, the catalyst activity was dramatically decreased and could not be reused for not more than three times [27]. When coated into SBA-15, alumina peptization under the acetic conditions could be deferred to some extent,

mainly owing to the interaction of alumina with SBA-15 silica and to the protection of SBA-15 host.

3.4. Spectroscopic characterization on the Pt/xAS catalysts

Based on the results and discussion mentioned above, the chirally-modified Pt/xAS catalysts were much better than Pt/SBA-15 catalyst, and showed better performance than the Pt/Al₂O₃ catalyst when the xAS composites had an alumina loading higher than 15 wt.%. In particular, the Pt catalysts supported on xAS composites prepared via an ultrasonic impregnation method behaved most actively among the Pt/xAS catalysts. In order to give some insights about the difference between the xAS composites prepared by different methods and to explain that why the Pt/xAS catalysts showed superior performance to the Pt/SBA-15 and Pt/alumina catalysts, the related catalysts were further characterized using relevant spectroscopic techniques.

The coordination state of Si in the xAS composites was directly characterized by ²⁹Si MAS NMR spectroscopy. Compared with the ²⁹Si MAS NMR spectrum of SBA-15, the Q3 signal was dramatically decreased while the Q4 was increased after alumina was coated into SBA-15 to form 25AS-UIW composites (see Fig. S6 in the Supplementary data). This may be resulted from transformation of Q3 to Q4 to form Si(OSi)₄ or Si(OSi)₃OAl [28]. Furthermore, the position of Q4 was shifted to ~107 ppm, demonstrating that part of aluminum was successfully inserted to the framework of SBA-15 to form Si-O-Al species. The IR spectra in the region of Si-OH and Al-OH stretching vibration of 25AS composites and Pt/25AS-UIW catalyst, after evacuation at an elevated temperature under vacuum, also confirmed the grafting of Al on surface silanol groups (see Fig. S7 in the Supplementary data). The intensity of surface silanol stretching vibration was markedly decreased after alumina was introduced whatever the method for preparation of xAS composites, compared with that of the SBA-15 host. After loading of Pt nanoparticles, the intensity of this bond was further decreased. A weak and broad shoulder between 3710 and 3735 cm⁻¹ centered at 3726 cm⁻¹ may reveal the presence of Al-OH groups.

The ²⁷Al MAS NMR spectroscopy was employed to extend characterization of the coordination state of Al in the xAS composites and some of Pt/xAS catalysts. As shown in Fig. S8 in the Supplementary data, all the samples mainly contained the tetrahedral Al^{IV} and octahedral Al^{VI} species [29]. In addition, for the xAS composites prepared by UIW and SIF methods, there were still Al^V species. Compared with Al₂O₃, the Al species signals shifted upfield (lower ppm values), indicating the coordination state of Al in the xAS composites was somewhat different from that in Al₂O₃. That is, in the xAS composites, Al not only coordinates with O atom to form the tetrahedral AlO₄, but also interacts with Si atom to form Al-O-Si species at the interface. This also infers that a part of aluminum in the xAS composites was inserted to the framework of SBA-15, in excellent agreement with the ²⁹Si NMR and IR results. Nevertheless, for xAS composites prepared by different methods, the relative ratios of Al^{IV} and Al^{VI} were also different. For the xAS-SSG composites, the Al^{IV} species were the dominant species; while for the xAS composites prepared by other methods, the Al^{VI} species were the main species. During preparation of xAS composites using SSG method, the instantaneous shear force can push Al atoms to insert the framework of SBA-15. Additionally, due to without competition of solvent during SSG process, Al salts can easily react with Si-OH to form Al-O-Si species. The coordination state of Al in the Pt/xAS catalysts did not change too much by comparison with their support composites.

It is widely accepted that the coordination state of Al is directly related to its acidity. The hydroxyl groups of the tetrahedral Al^{IV} will form Brönsted acidic sites (BAS); whereas dehydroxylation will give rise to Lewis acid sites (LAS). In order to detect the acidity of the xAS

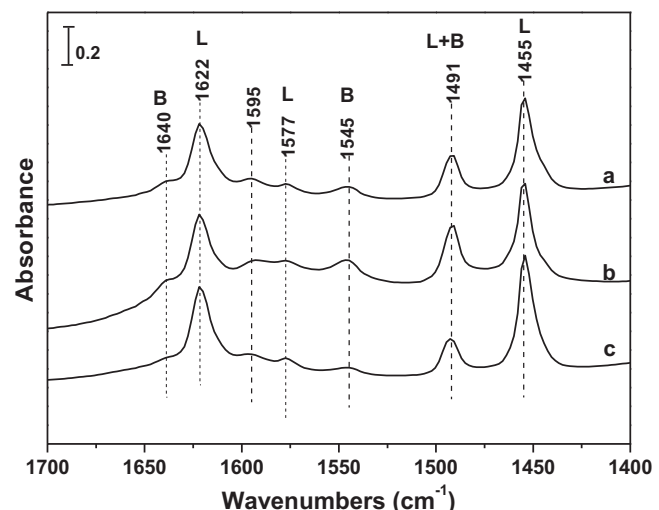


Fig. 4. IR spectra of pyridine adsorbed on (a) 25AS-SIH, (b) 25AS-SSG and (c) 25AS-UIW after evacuated at 573 K for 1 h.

composites and Pt/xAS catalysts, we extended the characterization of these samples by FT-IR spectroscopy using pyridine as probe molecules. Fig. 4 presents the IR spectra of pyridine adsorbed on the samples, after evacuation at 573 K for 1 h to remove gas-phase and physisorbed pyridine. Pyridine adsorbed on the xAS composites gave rise to IR bands at 1453, 1491, 1546, 1577, 1595, 1621 and 1639 cm⁻¹. The bands at 1453, 1491, 1577, and 1621 cm⁻¹ are attributed to pyridine coordinated with the LAS of the xAS composites, suggesting that the LAS originated from alumina were preserved [16]. The band at 1595 cm⁻¹ is associated with the adsorption of pyridine on alumina via a hydrogen bond. The weak IR bands at 1545 and 1640 cm⁻¹, detected for pyridine adsorbed on all the xAS composites, could be assigned to the protonation of pyridine (PyH⁺), indicating the presence of BAS. Qualitatively, the 25AS-SSG had more BAS amount; the 25AS-UIW had the highest L/B ratio, while the 25AS-SIH had the highest total amount of acid among all the xAS composites. The normalized peak areas for different xAS composites against the structure Si-O combination band at 1790–1930 cm⁻¹ are included in Table S1 in the Supplementary data. After Pt nanoparticles loading, the acid amount was decreased due to electron-donation of Pt nanoparticles to support [30].

The support materials would inevitably affect adsorption, dispersion and electronic properties of Pt nanoparticles on the support. The IR spectroscopic study of CO adsorption is the commonly used method to gain insight into the electronic properties and morphology of platinum. To help comparing our results to literature data, we extended the characterization of Pt/xAS catalysts with this method. To allow a direct comparison of these data with the catalytic results, the Pt/xAS catalysts were pretreated in a flowing H₂/Ar mixture at 673 K. Fig. 5 shows the DRIFT spectra of CO adsorbed on Pt/xAS catalysts. Only one mode of CO adsorption, linearly adsorbed CO, was identified. For CO linearly adsorbed on Pt/xAS catalysts, a broad band centered at 2064–2086 cm⁻¹ was observed. According to literatures, the signal can be split into two narrow intensive signals at ca. 2083 and 2064 cm⁻¹, and a broad band at ca. 2030 cm⁻¹. The first two signals are assigned to CO bound to highly coordinated Pt atoms such as (111) and (100) terraces, respectively, whereas the latter signal is attributed to CO adsorbed on low coordinated Pt sites at step-edges, corners and defects [31–35]. Sometimes, the stretching frequency for isolated CO species is influenced by the Pt dispersion [36]. The lower Pt dispersion, the higher stretching frequency.

For the CO adsorbed on pure alumina supported Pt/Al₂O₃ catalyst, an intensive band centered at 2065 cm⁻¹ was observed (Fig. 5f).

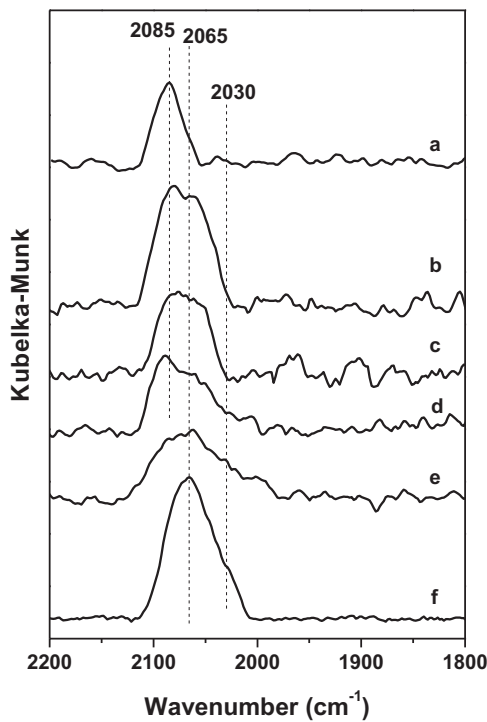


Fig. 5. DRIFT spectra of CO adsorbed at 308 K on the (a) Pt/25AS-SSG, (b) the Pt/25AS-UIW, (c) the Pt/25AS-SIW, (d) the Pt/25AS-SIH, (e) the Pt/35AS-SIF and (f) the $\text{Pt}/\text{Al}_2\text{O}_3$ catalyst.

After SBA-15 silica doped into alumina to form xAS composites, the stretching frequency for isolated CO species on the Pt/xAS catalysts shifted to higher wavenumbers. In particular, the IR band of CO linearly adsorbed on Pt/25AS-SSG was centered at 2085 cm^{-1} (Fig. 5a), about 20 cm^{-1} blue shift compared to that for $\text{Pt}/\text{Al}_2\text{O}_3$. In addition, the IR bands of CO linearly adsorbed on other Pt/xAS catalysts broadened a lot (Fig. 5b–e), especially for that on Pt/35AS-SIF catalyst (Fig. 5e). This suggests that there are many kinds of Pt species with different electronic properties or that there are Pt particles with different sizes to adsorb CO molecules, in good agreement with the TEM results. Actually, the Pt particle size of Pt/35AS-SIF catalyst was in the range of 1.0–8.0 nm, although the average size of 2.8 nm was calculated for this catalyst according to CO chemisorption. In contrast, the IR spectrum of CO adsorbed on Pt/25AS-UIW catalyst, which had a particle size distribution in the range of 1.0–4.0 nm, showed a relatively narrow peak (Fig. 5b). The blue shift of IR bands of CO adsorbed on Pt/xAS catalysts, in comparison with that on $\text{Pt}/\text{Al}_2\text{O}_3$ catalyst, further proved that the xAS composites had acidity, just like the literature reported data for $\text{Pt}/\text{Al}_2\text{O}_3\text{-SiO}_2$ catalyst involved in a similar asymmetric hydrogenation reaction [35].

Nevertheless, it is very difficult to make a simple correlation between the acidity and the blue shift of CO stretching frequency at this stage, because there are too many influencing factors to determine the stretching frequency of isolated CO species. In fact, the exact position of the CO absorption bands depends on the particle size [36] and surface coverage [37]. Furthermore, the shifts in the CO band position also probably reflect the changes in the electronic properties of Pt particles [38]. For a specific CO absorption band, the IR band at relatively higher position can also be attributed to CO linearly adsorbed on Pt particles with lower electron density dispersed on a support with stronger acidity. While the IR band centered at relatively lower position can be assigned to CO adsorbed on Pt particles with somewhat higher electron density dispersed on a support with weaker acidity. With increasing acidity of the support, the electronic charge of the support oxygen atoms to Pt atoms was

decreased and hence the electron density on the supported Pt particles was decreased [35,39]. This is in somewhat agreement with the pyridine adsorption IR results.

The representative Pt/xAS catalysts were further characterized using XPS in order to evaluate the surface properties of the Pt/xAS catalysts directly, after pretreated in a hydrogen flow at 673 K in a reactor attachment to XPS spectrometer. Due to that analysis of Pt supported on alumina containing materials by XPS is complicated by overlapping Al2p and Pt4f lines, the Pt4d lines are also used to eliminate the interference. As can be seen from Fig. S9A, although the Al2p and Pt4f signals are overlapped, the Pt4f lines can be deconvoluted easily owing to comparatively high Pt contents [40]. Correspondingly, the Pt4f_{7/2} positions of the Pt/xAS catalysts slightly varied with different preparation methods for the xAS composites. As listed in Table S2 in the Supplementary data, the binding energies for Pt4f_{7/2} of Pt/xAS catalysts were 71.1–71.2 eV. The surface Pt/Al atomic ratio (Pt/Al)_s was also calculated based on the Pt4f XPS results. Among the Pt/xAS catalysts, the Pt/25AS-UIW catalyst had the highest (Pt/Al)_s value of 0.022 with the lowest binding energy of Pt4f_{7/2}. The (Pt/Al)_s ratio was decreased as a order of Pt/25AS-UIW > Pt/35AS-SIF > Pt/25AS-SSG ≈ Pt/25AS-SIW > Pt/25AS-SIH. Fig. S9B in the Supplementary data shows the Pt4d lines of the Pt/xAS catalysts. Although these lines are relatively broad, only one surface Pt⁰ species can be deconvoluted from the raw data for all of Pt catalysts [40]. As also listed in Table S2 in the Supplementary data, the binding energy of Pt4d_{5/2} of 314.1 eV was the lowest for the Pt/25AS-UIW catalyst among the measured Pt catalysts.

3.5. Further discussion

To verify the influence of catalyst or support acidity on catalytic performance, we also carried out the chiral hydrogenation of EOPB in an aprotic solvent such as acetone. The Pt/25AS-SSG catalyst, of which the support was prepared by a solid-state grinding method, gave 83.1% conversion and 75.0% ee value, slightly lower than that obtained with the same catalyst in acetic acid (89.1% conversion and 78.3% ee). While for the $\text{Pt}/\text{Al}_2\text{O}_3$ catalyst, the conversion was decreased to less than a half in acetone compared with that obtained in acetic acid, and the ee value was also decreased notably to 60%. That is, in acetone, the gap between the catalytic performance obtained with $\text{Pt}/\text{Al}_2\text{O}_3$ and Pt/25AS-SSG catalyst was further expanded. As we have already known, in acetic acid, the basic N atom of chiral modifier cinchonidine can be protonated and these chemical changes influence the reaction rate and enantioselectivity. While in acetone, the improvement by the protonation of basic N atom of chiral modifier could be excluded owing to aprotic solvent. Nevertheless, the support acidity of the composites affects the electronic state of Pt and thus influences the enantioselectivity and reaction rate [35,41]. Based on the IR characterizations, the 25AS-UIW composites had more acid amount than the 25AS-SSG, thus the former supported Pt catalyst behaved more actively than the latter supported one in the enantioselective hydrogenation of EOPB. Although Al_2O_3 also contained LAS, the lower specific surface area compared with the xAS composites would result in a lower specific surface density of LAS in terms of alumina weight [39]. While a higher surface density of acid sites on the support will be beneficial for dispersion of Pt nanoparticles and for adsorption of EOPB, as a result, higher catalytic performance can be acquired from the xAS composites supported Pt catalyst [42]. In the interpretation of the metal-support interaction, it is commonly assumed that the shift in the electronic properties of Pt with support acidity controls the characteristics of the Pt-H system [43,44].

Moreover, introduction of alumina inside the mesoporous channels of SBA-15 can protect alumina from peptization in acetic acid effectively. Therefore, the reusability of the Pt/xAS catalysts was

greatly improved compared with the bare alumina supported Pt catalyst. The Pt/35AS-UIW catalyst could be reused at least for seven times without obvious loss in activity or enantioselectivity. Ultrasonic irradiation cannot only make alumina precursor disperse uniformly inside the mesopores of SBA-15, but also enhance the interaction between SBA-15 silica and alumina [45]. Although there was slight aggregation of Pt nanoparticles after several recycles, the used Pt/35AS-UIW catalyst also had a dispersion of higher than 30%. Additionally, it is worth noting that the different (Pt/Al)s values also indicate that on the surface of Pt/xAS catalysts, there were different amount of Pt atoms participating in the chiral hydrogenation of EOPB. The Pt/25AS-UIW catalyst bears a highest Pt/Al ratio, so that the highest conversions and ee values were obtained with this catalyst under the same conditions. In a word, what makes Pt/xAS-UIW catalysts, the most active ones, special should be surface acidity, Pt particle size and adsorptive properties.

4. Conclusions

$\text{Al}_2\text{O}_3@\text{SBA-15}$ composites with different alumina loadings were prepared via different routes. The $\text{Al}_2\text{O}_3@\text{SBA-15}$ composites not only retained the ordered mesostructure of the SBA-15 host, but also showed the different surface chemical nature from the pure Al_2O_3 or SBA-15 silica. The $\text{Al}_2\text{O}_3@\text{SBA-15}$ composites were proved to be remarkable supports for Pt nanoparticles towards the enantioselective hydrogenation of ethyl 2-oxo-4-phenylbutyrate after chirally modified with chiral modifier cinchonidine. Compared with pure alumina or SBA-15 silica supported Pt catalysts, the Pt/ $\text{Al}_2\text{O}_3@\text{SBA-15}$ catalysts showed superior results if the alumina loading in the composites reached above 15 wt.%. Owing to protection of SBA-15 silica wall, the alumina located inside the mesopores can resist peptization in acetic acid for much longer time, so that the reusability of the Pt/ $\text{Al}_2\text{O}_3@\text{SBA-15}$ catalysts was greatly improved by comparison with that of Pt/ Al_2O_3 catalyst under the same conditions.

It is worth noting that among all the Pt catalysts, the Pt catalysts supported on $\text{Al}_2\text{O}_3@\text{SBA-15}$ composites prepared by an ultrasonic impregnation method were most active due to uniformly dispersed alumina and strong interaction of alumina with SBA-15 silica. Up to $11,928 \text{ h}^{-1}$ TOF and 87.9% ee value were achieved under the optimal reaction conditions. Based on the spectroscopic characterizations for the representative Pt catalysts, we deduce that Pt particle size and dispersion, electronic properties of Pt particles, and support acidity would affect the catalytic performance in a comprehensive manner. This kind of catalyst may provide a potential alternative for the hydrogenation of other compounds containing carbonyl groups such as α,β -unsaturated aldehydes.

Acknowledgments

This work was supported by the National Natural Science Foundation of China (NSFC Grant Nos. 21273076 and 21373089), the Open Research Fund of Top Key Discipline of Chemistry in Zhejiang Provincial Colleges (ZJHX2013) and Key Laboratory of the Ministry of Education for Catalysis Materials (Zhejiang Normal University), Programs Foundation of Ministry of Education of the People's Republic of China (2012007613000), and Shanghai Leading Academic Discipline Project (B409). Finally, helpful comments have been made by the reviewers, and some of these were followed in the revision.

Appendix A. Supplementary data

Supplementary data associated with this article can be found, in the online version, at <http://dx.doi.org/10.1016/j.apcata.2014.09.027>.

References

- [1] T. Mallat, E. Orglmeister, A. Baiker, *Chem. Rev.* 107 (2007) 4863.
- [2] M. Studer, H.U. Blaser, C. Exner, *Adv. Synth. Catal.* 345 (2003) 45.
- [3] M. Bartok, *Curr. Org. Chem.* 10 (2006) 1533.
- [4] Y. Orito, S. Imai, S. Niwa, *Preprints of the 43rd Catalysis Forum, Japan*, 1978, pp. 130.
- [5] Y. Orito, S. Imai, S. Niwa, *Bull. Chem. Soc. Jpn.* 52 (1979) 1118.
- [6] Y. Orito, S. Imai, S. Niwa, *Bull. Chem. Soc. Jpn.* 55 (1982) 137.
- [7] S. Basu, M. Mapa, C.S. Gopinath, M. Doble, S. Bhaduri, G.K. Lahiri, *J. Catal.* 239 (2006) 154.
- [8] F. Meemken, A. Baiker, J. Dupre, K. Hungerbuhler, *ACS Catal.* 4 (2014) 344.
- [9] G. Martin, P. Maki-Arvela, D.Y. Murzin, T. Salmi, *Catal. Sci. Technol.* 4 (2014) 170.
- [10] Q. Li, X. Zhang, M. Xiao, Y. Liu, *Catal. Commun.* 42 (2013) 68.
- [11] H. Pan, X. Li, D. Zhang, Y. Guan, P. Wu, *J. Mol. Catal. A* 377 (2013) 108.
- [12] M.Y. Kim, S.B. Jung, M.G. Kim, Y.S. You, J.H. Park, C.H. Shin, G. Seo, *Catal. Lett.* 129 (2009) 194.
- [13] M.J. Beier, J.-M. Andanson, T. Mallat, F. Krumeich, A. Baiker, *ACS Catal.* 2 (2012) 337.
- [14] N. Erathodiyil, H. Gu, H. Shao, J. Jiang, J.Y. Ying, *Green Chem.* 13 (2011) 3070.
- [15] B. Li, X. Li, Y. Ding, P. Wu, *Catal. Lett.* 142 (2012) 1033.
- [16] H. Wang, X. Li, Y.M. Wang, P. Wu, *Catal. Chem. Eng.* 2 (2010) 1303.
- [17] Z. Chen, Z. Guan, M. Li, Q. Yang, C. Li, *Angew. Chem. Int. Ed.* 50 (2011) 4913.
- [18] D. Zhao, J. Feng, Q. Huo, N. Melosh, G.H. Fredrickson, B.F. Chmelka, G.D. Stucky, *Science* 279 (1998) 548.
- [19] J.M. Du, H.L. Xu, J. Shen, J. Huang, W. Shen, D. Zhao, *Appl. Catal. A* 296 (2005) 186.
- [20] Z. Luan, M. Hartmann, D. Zhao, W. Zhou, L. Kevan, *Chem. Mater.* 11 (1999) 1621.
- [21] Y. Li, Y. Chen, L. Li, J. Gu, W. Zhao, L. Li, J. Shi, *Appl. Catal. A* 366 (2009) 57.
- [22] R. Ryoo, S. Jun, J.M. Kim, M.J. Kim, *Chem. Commun.* (1997) 2225.
- [23] X. Li, Y. Shen, R. Xing, Y. Liu, H. Wu, M. He, P. Wu, *Catal. Lett.* 122 (2008) 325.
- [24] Q. Li, Z. Wu, B. Tu, S.S. Park, C.-S. Ha, D. Zhao, *Micropor. Mesopor. Mater.* 135 (2010) 95.
- [25] T. Tsioncheva, L. Ivanova, J. Rosenholm, M. Linden, *Appl. Catal. B* 89 (2009) 365.
- [26] M.R. Attwood, C.H. Hassall, A. Krohn, G. Lawton, S. Redshaw, *J. Chem. Soc. Perkin Trans. I* (1986) 1011.
- [27] B. Li, X. Li, H. Wang, P. Wu, *J. Mol. Catal. A* 345 (2011) 81.
- [28] W. Kolodziejek, A. Corma, M.-T. Navarro, J. Perez-Pariente, *Solid State Nucl. Magn. Reson.* 2 (1993) 253.
- [29] Z. Luan, C. Cheng, W. Zhou, J. Klinowski, *J. Phys. Chem.* 99 (1995) 1018.
- [30] B.C. Beard, Z.C. Zhang, *Catal. Lett.* 82 (2002) 1.
- [31] M.J. Kappers, J.H. van der Maas, *Catal. Lett.* 10 (1991) 365.
- [32] E. Schmidt, W. Kleist, F. Krumeich, T. Mallat, A. Baiker, *Chem. Eur. J.* 16 (2010) 2181.
- [33] K. McCrea, J.S. Parker, P. Chen, G. Somorjai, *Surf. Sci.* 494 (2001) 238.
- [34] H. Harle, U. Metka, H.-R. Volpp, J. Wolfrum, *Phys. Chem. Chem. Phys.* 1 (1999) 5059.
- [35] E. Hoxha, B. Schimmoeller, Z. Cakl, A. Urakawa, T. Mallat, S.E. Pratsinis, A. Baiker, *J. Catal.* 271 (2010) 115.
- [36] L.-C. de Menorval, A. Chaqroune, B. Coq, F. Figueras, *J. Chem. Soc. Faraday Trans.* 93 (1997) 3715.
- [37] F. Stoop, F.J.C.M. Toolenaar, V. Ponec, *J. Catal.* 73 (1982) 50.
- [38] G. Blyholder, *J. Phys. Chem.* 68 (1964) 2772.
- [39] S. Handjani, E. Marceau, J. Blanchard, J.-M. Krafft, M. Che, P. Mäki-Arvela, N. Kumar, J. Wärna, D. Yu Murzin, *J. Catal.* 282 (2011) 228.
- [40] J.Z. Shyu, K. Otto, *Appl. Surf. Sci.* 32 (1988) 246.
- [41] S. Bottcher, C. Hoffmann, K. Rauchle, W. Reschetilowski, *ChemCatChem* 3 (2011) 741.
- [42] B. Schimmoeller, F. Hoxha, T. Mallat, F. Krumeich, S.E. Pratsinis, A. Baiker, *Appl. Catal. A* 374 (2010) 48.
- [43] Y. Ji, V. Koot, A.M.J. van der Eerden, B.M. Weckhuysen, D.C. Koningsberger, D.E. Ramaker, *J. Catal.* 245 (2007) 415.
- [44] A.Y. Stakheev, Y. Zhang, A.V. Ivanov, G.N. Baeva, D.E. Ramaker, D.C. Koningsberger, *J. Phys. Chem. C* 111 (2007) 3938.
- [45] B. Torok, G. Szollosi, K. Balazsik, K. Felfoldi, I. Kun, M. Bartok, *Ultrason. Sonochem.* 6 (1999) 97.